

Configuration Effects of H-Bonded Sites and Rigid Core Lengths on H-Bonded Banana-Shaped Liquid Crystalline Supramolecules Consisting of Symmetric Trimers and Asymmetric Heterodimers

Ling-Yung Wang,[†] I-Hung Chiang,[†] Po-Jen Yang,[†] Wan-Sheung Li,[‡] I-To Chao,[‡] and Hong-Cheu Lin^{*,†}

Department of Materials Science and Engineering, National Chiao Tung University, Hsinchu, Taiwan (ROC),
Institute of Chemistry, Academia Sinica, Taipei, Taiwan (ROC)

Received: July 31, 2009; Revised Manuscript Received: September 3, 2009

Several series of novel banana-shaped H-bonded symmetric trimers (with two H-bonds) and asymmetric heterodimers (with one H-bond) were self-assembled by appropriate molar ratios of proton donors (H-donors) and acceptors (H-acceptors). The influences of H-bonded linking positions and aromatic ring numbers (4–8 aromatic rings in the rigid cores) as well as the chain lengths (n , $m = 12$ or 16 , respectively, in the flexible parts) on the mesomorphism and the switching behavior of the bent-core supramolecules were evaluated and theoretically analyzed. Except for the supramolecular structures with longer rigid cores or shorter flexible chains possessing the rectangular columnar (Col_r or B1) phase, the SmC_AP_A phase was revealed in most supramolecular asymmetric heterodimers and switched to the SmC_SP_F phase by applying electric fields. The polar smectic C phase was dominated for those with H-bonded sites apart from the core center. Interestingly, the SmA and nematic phases were observed in H-bonded asymmetric dimers with H-bonded sites close to the core center, which theoretically proved that the polar smectic C phase was disfavored due to an unfavorable bend angle (smaller than the lower limit of 110°) in the lowest-energy H-bonded conformer. Compared with the fully covalently bonded analogue, lower transition temperatures and lower threshold voltages were developed in the H-bonded asymmetric dimers with the polar smectic C phase. On the basis of the theoretical calculations of molecular modeling, the existence of polar switching behavior in the polar smectic C phase of asymmetric heterodimers was proven to be associated with their configurations with higher dipole moments and suitable bend angles. Furthermore, the lack of polar switching behavior in supramolecular symmetric trimers, which exhibited the regular SmC phase with weak electrical stabilities, was related to their configurations with smaller dipole moments and confirmed by theoretical calculations.

Introduction

The concept of supermolecules bearing noncovalent bond segments (e.g., hydrogen-bonds (H-bonds)) was investigated and developed because of its functional properties and extensive availabilities by the molecular design of inter- or intramolecular configurations. Self-assembled phenomena through molecular recognition between complementary constituents have been explored in various areas, such as biomaterials, liquid crystalline (LC) materials, and materials for electrooptical applications.¹ Interestingly, supramolecular approaches have been employed recently in mesomorphic studies to establish self-assembled molecules, such as H-bonded mesogens.² Ferroelectric and antiferroelectric liquid crystals (FLCs and AFLCs) become more important due to their fast response of electrooptical properties by applying external electric fields.³ At early stages, the molecular design of FLCs was confined to molecular structures having chiral centers. However, since the first example of the achiral bent-core (banana-shaped) mesogen possessing switchable behavior was explored,⁴ many kinds of bent-core liquid crystals have been synthesized to examine their mesomorphic and electrooptical properties.

Regarding single bent-core molecules with low molecular weights, the configuration effects, such as various rigid core shapes, flexible chain lengths, and substituents at different positions of rigid cores, have been studied, as well.⁵ Furthermore, bent-core molecules with rodlike rigid units attached to one end of the terminal flexible chains⁶ and special bent-core structures connected to silicon groups at the centers or the termini of the flexible chains⁷ were inspected. In addition, polymeric,⁸ dimeric,⁹ and dendritic bent-core molecules¹⁰ also have been developed. Hence, detailed studies of banana-shaped molecules with bent-core structures connected by normal covalent bonds have been surveyed thoroughly. In recent years, the supramolecular bent-core model in which two complementary segments are linked through H-bonds has been explained.¹¹ One H-bonded bent-core system formed by oxadiazole mesogens was developed and only the SmA phase without switching behavior was exhibited.¹² So far, few records regarding H-bonded banana-shaped liquid crystals with given fundamental electric and optical behavior have been reported, and their analogous side-chain polymers were developed by Serrano's group.¹³ However, the comprehensive influences of the number and site of H-bonds on the spontaneous polarization and switching current behavior of banana-shaped liquid crystalline supramolecules are lacking. In addition, the influence of H-bonds on the threshold voltages of (anti)ferroelectric switching phenomena and the investigation of dipole moment and bend

* Corresponding author. Phone: 8863-5712121, ext. 55305. Fax: 8863-5724727. E-mail: linhc@cc.nctu.edu.tw.

[†] National Chiao Tung University.

[‡] Academia Sinica.

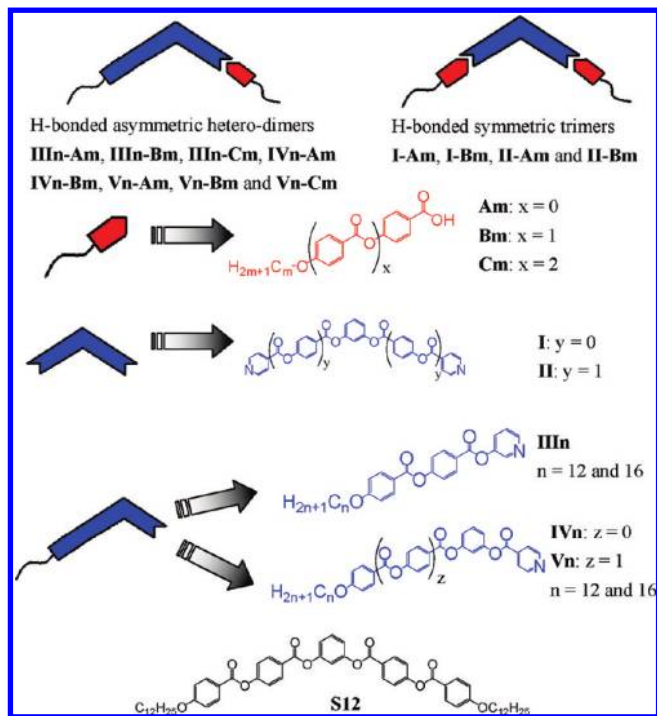


Figure 1. Chemical structures of fully covalently bonded five-ring bent-core molecule **S12**,¹³ H-bonded bent-core symmetric trimers, and asymmetric dimers containing acidic H-donors (**Am**, **Bm**, and **Cm**) and pyridyl H-acceptors (**I–II** and **III_n–V_n**).

angle effects on polar switching behaviors in H-bonded bent-core supramolecules have still not been reported.

Herein, to investigate the influence of H-bonded configurations (H-bonded linking positions, the aromatic ring numbers, and the chain lengths) in molecular skeletons on mesomorphic and the electrooptical properties of bent-core structures, several series of novel banana-shaped supramolecules consisting of H-bonded symmetric trimers (with two H-bonds) and asymmetric heterodimers (with one H-bond) were self-assembled by appropriate molar ratios of proton donors (H-donors) and acceptors (H-acceptors). Three kinds of acidic H-donors (**Am**, **Bm**, and **Cm**) and five kinds of bent-core H-acceptors (**I–II** and **III_n–V_n**, bearing double and single terminal pyridyl groups, respectively) were synthesized and are displayed in Figure 1. H-bonded symmetric supramolecules were self-assembled by bis-pyridyl H-acceptors (**I–II**) with acidic H-donors (**Am** and **Bm**) to form trimers (with two H-bonds), where acidic H-donor **Cm** was not used due to the superhigh transition temperatures of their supramolecules consisting of **Cm** and H-acceptors (**I–II**). H-bonded asymmetric supramolecules were self-assembled by single-pyridyl H-acceptors (**III_n–V_n**) with acidic H-donors (**Am**, **Bm**, and **Cm**) to form heterodimers (with one H-bond). In contrast to the fully covalently bonded structures, the H-bonded effects of H-bonded symmetric trimers (with two H-bonds) and asymmetric heterodimers (with one H-bond) with analogous H-bonded configurations with mesomorphic and electrooptical properties were investigated. The mesomorphic and electrooptical properties of all H-bonded complexes were examined and surveyed by polarizing optical microscopy (POM), differential scanning calorimetry (DSC), powder X-ray diffraction (XRD) measurements, and electrooptical switching experiments. The variation of polar switching behavior for H-bonded symmetric trimers and asymmetric heterodimers were evaluated by the theoretical calculation of electron cloud dispersions, dipole moments, and bend angles.

Experimental Section

Characterization Methods. ¹H NMR spectra were recorded on a Varian Unity 300 MHz spectrometer using DMSO-*d*₆ and CDCl₃ as solvents. Mass data were measured by a Micromass TRIO-2000 GC/MS. Elemental analyses were performed on a Heraeus CHN-OS RAPID elemental analyzer. Mesophasic textures were characterized by polarizing optical microscopy using a Leica DMLP equipped with a hot stage. Infrared (IR) spectra were investigated by a Perkin-Elmer Spectrum 100 instrument. Temperatures and enthalpies of phase transitions were determined by differential scanning calorimetry (model: Perkin-Elmer Pyris 7) under N₂ at a heating and cooling rate of 5 °C min⁻¹. Synchrotron powder X-ray diffraction measurements were performed at beamline BL17A of the National Synchrotron Radiation Research Center (NSRRC), Taiwan, where the wavelength of the X-ray was 1.334 431 Å. The XRD data were collected using imaging plates (area = 2 × 40 cm² and a pixel resolution of 100) curved with a radius equivalent to a sample-to-image plate distance of 280 mm, and the diffraction signals were accumulated for 3 min. The powder samples were packed into a capillary tube and heated by a heat gun, for which the temperature controller is programmable by a PC with a PID feedback system. The scattering angle, θ , was calibrated by a mixture of silver behenate and silicon. The electrooptical properties were determined in commercially available ITO cells (from Mesostate Corp., thickness = 4.25 μm, active area = 1 cm²) with rubbed polyimide alignment coatings (parallel rubbing direction). A digital oscilloscope (Tektronix TDS-3012B) was used in these measurements, and a high-power amplifier connected to a function generator (GW model GFG-813) with a dc power supply (Keithley 2400) was utilized in the dc field experiments. During electrooptical measurements, the modulations of textures by applying electric fields were observed by POM. The dielectric permittivity studies were investigated by an impedance/gain-phase analyzer (HP41-94A) in nonrubbing cells with a cell gap of 9 μm at a frequency of 5 kHz and various cooling temperatures.

Computational Method. Sets of low-energy structures were obtained from a systematic pseudo Monte Carlo search using MacroModel V 9.5 with an all-atom amber* force field in the gas phase on each bent-core structure of **S1**, **I–A1**, **IV1–A1**, and **III1–B1**.¹⁴ Five thousand structures were sampled (with an energy window of 5 kcal/mol) for each search, and they were minimized using a PR conjugated gradient method to obtain the lowest-energy structure in each simulation. Unique conformations within 1 kcal/mol of the global minimum were used in full geometry optimization using Gaussian03 at the B3LYP level with the 6-31G(d) basis set.¹⁵

Synthesis. All synthetic processes were followed according to the five routes shown in Scheme S1 (see the Supporting Information). The esterification reactions were carried out via two procedures (i.e., steps i and iii) to acquire related products. Protecting reactions proceeded via step iv. Deprotecting actions were executed by two procedures (i.e., steps ii and v) to eliminate the protecting groups. In addition, the starting compounds **Am** ($m = 12$ and 16) were prepared according to the literature procedures,¹⁶ and all synthetic details are described in the Supporting Information.

Sample Preparation. All H-bonded complexes were constructed by mixing appropriate molar ratios of proton donors and acceptors in solutions of chloroform/THF (~1:1 vol), which were self-assembled into supramolecules by evaporating solvents slowly. Several series of H-bonded, bent-core structures with 4–8 aromatic rings were formed in two types of configurations:

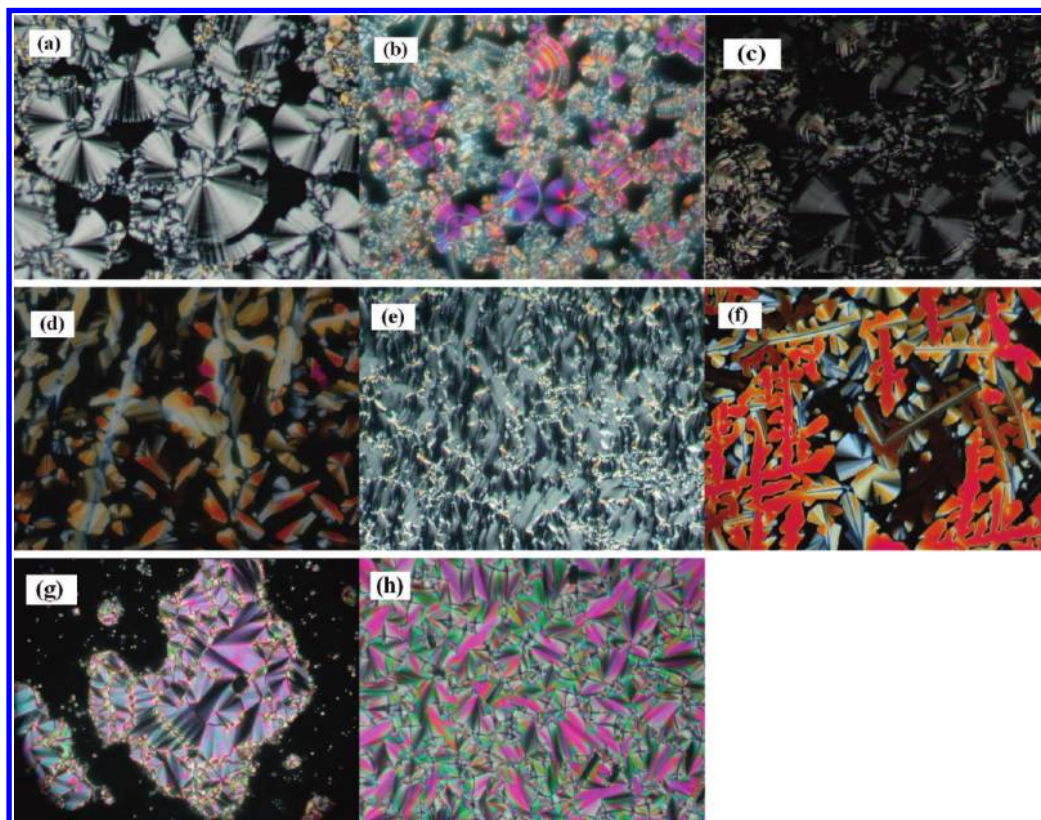


Figure 2. POM textures at the cooling process: (a) the polar smectic phase with the spherulite texture of complex **IV12-A12** at 96 °C; (b) the polar smectic phase with spherulite and nonspecific grainy textures of complex **IV12-B16** at 100 °C; (c) the polar smectic phase with spherulite and stripe textures of complex **V12-A12** at 100 °C; (d) the Col_r phase with dendritic- and mosaic-like textures of complex **V12-B12** at 120 °C; (e) the polar smectic phase with the fanlike texture of complex **V16-B16** at 140 °C; (f) the Col_r phase with dendritic- and mosaic-like textures of complex **V12-C12** at 130 °C; (g) the smectic A phase with the fanlike texture of complex **III16-B16** at 110 °C. (h) the smectic A phase with the fanlike texture of complex **III16-A16** at 95°.

(i) asymmetric heterodimers (with one H-bond) consisting of single-pyridyl H-acceptors (**III_n-V_n**, where $n = 12$ and 16) with acidic H-donors (**Am**, **Bm**, and **Cm**, where $m = 12$ and 16) and (ii) H-bonded symmetric trimers (with two H-bonds) consisting of bis-pyridyl H-acceptors (**I-II**) with acidic H-donors (**Am** and **Bm**, where $m = 12$ and 16).

Results and Discussion

Mesophasic and Thermal Properties of H-Bonded Asymmetric Heterodimers (with One H-Bond). (i) *Four- and Five-Ring Systems (III_n-Am, III_n-Bm, and IV_n-Am).* To understand the influence of H-bonded sites (at the rigid cores) on mesomorphism, molecular stacking, and thermal properties, H-bonded four- and five-ring asymmetric heterodimers (i.e., **III_n-Am**, **III_n-Bm**, and **IV_n-Am** ($n, m = 12$ and 16 , respectively)), were investigated by POM and DSC measurements. In addition, an analogous fully covalently bonded structure **S12** ($n = 12$) with five rings (see Figure 1), which has been reported by Pelzl et al.,¹⁷ was compared, as well. Furthermore, their mesophasic textures, phase transition temperatures, and enthalpy values are shown in Figure 2a, g, h, Figure 3a, and Table 1. All complexes **III_n-Am** and **III_n-Bm** ($n, m = 12$ and 16 , respectively) possessed the smectic A (SmA) phase, which was verified by POM to show the enantiotropic fanlike texture. For instance, the fanlike texture of complexes **III16-A16** and **III16-B16** are demonstrated in Figure 2h and g, respectively. However, complexes **IV_n-Am** revealed a polar smectic (B2 or SmCP) phase¹⁸ in both heating and cooling processes, and the POM texture of complex **IV12-A12** is shown in Figure 2a.

Regarding H-bonded four- and five-ring asymmetric heterodimers **III_n-Am** and **III_n-Bm** with different bent-core lengths (4 and 5 rings) but the same near-central H-bonded sites at the rigid cores, complexes **III_n-Bm** bearing longer bent-core lengths (5 rings) possessed higher phase transition temperatures and broader SmA phase ranges than analogous complexes **III_n-Am** (4 rings). To compare the mesophasic type of five-ring complexes **III_n-Bm** and **IV_n-Am** with different H-bonded sites at the rigid cores, the SmCP and SmA mesophases were achieved for supramolecular mesogens with far- and near-central H-bonded sites, respectively. This phenomenon suggested that the polar smectic phase would be preferred if the H-bonded site was far away from the bent-core center in supramolecular design, which means the higher stability of the SmCP phase was induced by longer covalently bonded bent cores of **IV_n** in complexes **IV_n-Am**. Moreover, the isotropization temperatures of complexes **III_n-Bm** are higher than those of complexes **IV_n-Am** due to the relatively higher isotropization temperatures of H-donors **Bm** with longer rigid cores in analogous **Am** and **Bm** ($m = 12$ and 16). In comparison with analogous compound **S12**, complexes **IV_n-Am** show lower phase transition temperatures and similar mesophasic ranges.

(ii) *Six-Ring Systems (III_n-Cm, IV_n-Bm, and V_n-Am).* Three series of comparable six-ring asymmetric heterodimers (i.e., **III_n-Cm**, **IV_n-Bm**, and **V_n-Am** ($n, m = 12$ and 16 , respectively)), were investigated for the influence of different H-bonded sites (at the rigid cores) on their mesophasic types and phase transition temperatures, as shown in Table 2 and

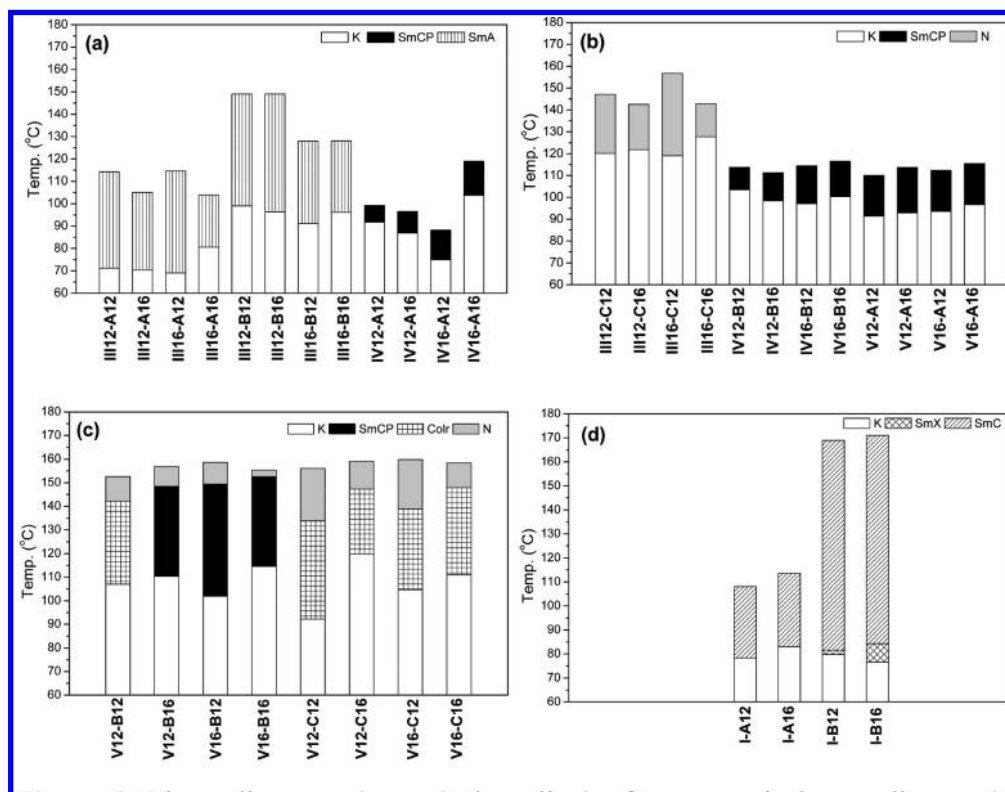


Figure 3. Phase diagrams (upon second cooling) of asymmetric heterodimers: (a) four- and five-ring systems (**III_n-Am**, **III_n-Bm**, and **IV_n-Am**); (b) six-ring systems (**III_n-Cm**, **IV_n-Bm**, and **V_n-Am**); (c) seven- and eight-ring systems (**V_n-Bm** and **V_n-Cm**), and symmetric trimers; (d) five- and seven-ring systems (**I-Am** and **II-Am**).

Figure 3b. With respect to the mesophasic types, the entropic nematic phase was obtained in complexes **III_n-Cm** ($n, m = 12$ and 16 , respectively) with near-central H-bonded sites (at the rigid cores) to indicate their loose molecular stackings, but analogous complexes **IV_n-Bm** and **V_n-Am** ($n, m = 12$ and 16 , respectively) exhibited SmCP phases owing to their far-central H-bonded sites, whose trends are the same as five-ring asymmetric heterodimers **IV_n-Am** with H-bonded sites far away from the bent-core centers. The mesophasic textures were examined by POM experiments. For instance, complex **IV12-B16** reveals spherulite and nonspecific grainy textures in Figure 2b, and complex **IV12-A12** exhibited spherulite and stripe textures in Figure 2c, which suggested the polar smectic (SmCP) phase.

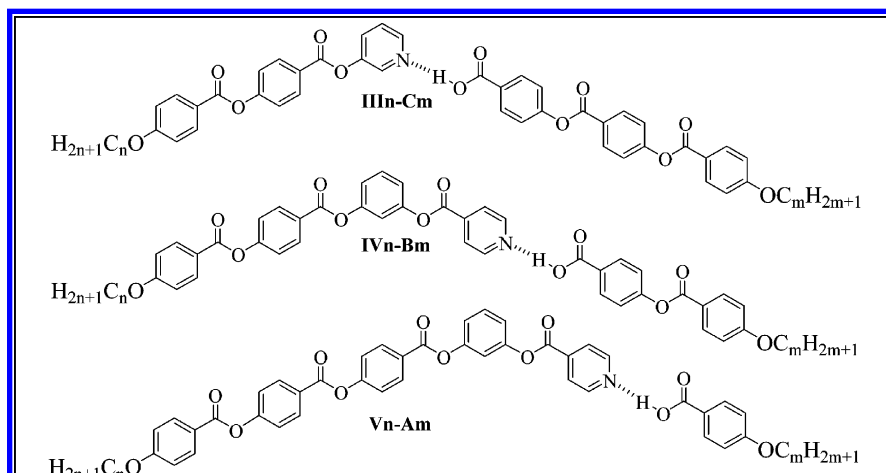
Comparing the phase transition temperatures of six-ring asymmetric heterodimers **III_n-Cm**, **IV_n-Bm**, and **V_n-Am** (Figure 3b), complexes **III_n-Cm** revealed the highest isotropization temperatures due to the relatively much higher isotropization temperatures of ingredients in H-donors **Cm** with the longest rigid cores (see Supporting Information Figure S1 and Table S1) in analogous **Am**, **Bm**, and **Cm** ($m = 12$ and 16). Similar phenomena were also displayed for isotropization temperatures of five-ring complexes **III_n-Bm** and **IV_n-Am**. Meanwhile, the SmCP phase ranges of **V_n-Am** are slightly wider than those of **IV_n-Bm**, which might be due to the higher stability of the SmCP phase caused by longer covalently bonded bent cores of **V_n** in complexes **V_n-Am**.

(iii) *Seven- and Eight-Ring Systems (IV_n-Cm, V_n-Bm, and V_n-Cm).* Three series of H-bonded seven- and eight-ring asymmetric heterodimers (i.e., **IV_n-Cm**, **V_n-Bm**, and **V_n-Cm** ($n, m = 12$ and 16 , respectively)), were investigated for the influence of different H-bonded sites (at the rigid cores) and ring numbers on their mesophasic types and phase transition

TABLE 1: Phase Transition Temperatures and Enthalpies of H-Bonded Four- and Five-Ring Asymmetric Hetero-Dimers (with One H-Bond)^a

Complex	n	m	x	Phase transition temperature/°C [Enthalpy/kJ/g]				
III12-A12	12	12	1	I	114.3 [20.5]	SmA	71.2 [69.8]	K
III12-A16	12	16	1	I	105.0 [14.0]	SmA	70.4 [152.1]	K
III16-A12	16	12	1	I	114.6 [25.0]	SmA	69.1 [49.3]	K
III16-A16	16	16	1	I	103.9 [14.3]	SmA	80.6 [146.5]	K
III12-B12	12	12	2	I	149.0 [7.5]	SmA	99.0 [161.2]	K
III12-B16	12	16	2	I	149.1 [9.6]	SmA	96.3 [169.8]	K
III16-B12	16	12	2	I	128.0 [10.8]	SmA	91.2 [135.0]	K
III16-B16	16	16	2	I	128.1 [8.2]	SmA	96.2 [157.2]	K
IV12-A12	12	12	—	I	99.2 [27.1]	CmCP	91.7 [22.3]	K
IV12-A16	12	16	—	I	96.5 [21.3]	CmCP	86.9 [30.1]	K
IV16-A12	16	12	—	I	88.2 [17.2]	CmCP	75.0 [33.4]	K
IV16-A16	16	16	—	I	119.0 [20.7]	CmCP	103.7 [54.1]	K

^a I = isotropic state; SmA = smectic phase with no (or less) tilt angle arrangements; SmCP = polar tilt smectic phase; K = crystalline state. The phase transitions were measured by DSC at the 2nd cooling scan with a cooling rate of 5 °C min^{-1} . Phase transitions of compound **S12** were obtained as I 119.0 [22.5] CmCP 109.0 [41.9] K, which were reported by Pelzl et al.¹³

TABLE 2: Phase Transition Temperatures and Enthalpies of H-Bonded Six-Ring Asymmetric Heterodimers (with One H-Bond)^a


Complex	n	m	Phase transition temperature/°C [Enthalpy/kJ/g]				
III12-C12	12	12	I	147.2 [20.3]	N	120.1 [2.7]	K
III12-C16	12	16	I	142.6 [25.0]	N	121.8 [2.3]	K
III16-C12	16	12	I	156.7 [17.8]	N	119.1 [3.6]	K
III16-C16	16	16	I	142.9 [11.9]	N	127.7 [3.1]	K
IV12-B12	12	12	I	113.8 [32.7]	SmCP	103.4 [64.1]	K
IV12-B16	12	16	I	111.3 [20.0]	SmCP	98.4 [50.7]	K
IV16-B12	16	12	I	114.4 [34.4]	SmCP	97.2 [82.6]	K
IV16-B16	16	16	I	116.5 [30.7]	SmCP	100.4 [98.2]	K
V12-A12	12	12	I	110.0 [19.6]	SmCP	91.4 [43.6]	K
V12-A16	12	16	I	113.7 [27.1]	SmCP	92.8 [39.4]	K
V16-A12	16	12	I	112.4 [22.8]	SmCP	93.6 [59.9]	K
V16-A16	16	16	I	115.5 [28.5]	SmCP	96.6 [72.3]	K

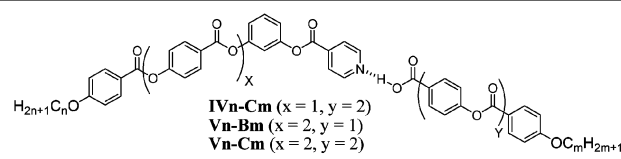
^a I = isotropic state; N = nematic phase; SmCP = polar tilt smectic phase; K = crystalline state. The phase transitions were measured by DSC at the 2nd cooling scan with a cooling rate of 5 °C min⁻¹.

temperatures, as shown in Table 3 and Figure 3c. Due to the large variation of solubilities in H-donors **Cm** and H-acceptors **IVn**, phase separation occurred in the preparation of complexes **IVn-Cm**, so these complexes could not be compared in this study. In regard to the mesophasic types, the nematic phase was observed in both series of complexes **Vn-Bm** and **Vn-Cm**. In addition, the rectangular columnar (Col_r or B1) and SmCP phases were obtained in complexes **Vn-Bm** (**n, m** = 12 and 16, respectively) with seven rings (at the rigid cores), where complex **V12-B12** demonstrated the Col_r phase due to its shorter flexible chain length (**n, m** = 12). However, analogous complexes **Vn-Cm** (**n, m** = 12 and 16) with eight rings (at the rigid cores) exhibited only the Col_r phase owing to their longer rigid cores, in contrast to complexes **Vn-Bm** (with seven rings). The mesophasic textures were evidenced by POM experiments. For example, complex **V16-B16** displayed the fanlike texture in Figure 2e as evidence of the polar smectic (SmCP) phase, and complexes **V12-B12** and **V12-C12** exhibited dendritic-like and mosaic-like textures in Figure 2d and f, which were the symbolic textures of the Col_r phase. In general, complexes **Vn-Cm** (with eight rings) had higher transition temperatures and wider nematic phase ranges than **Vn-Bm** (with seven rings), in which the wider nematic phase

ranges in complexes **Vn-Cm** is due to their higher length ratios of rigid cores (with eight rings) to flexible chains.

Overall, comparing all H-bonded asymmetric heterodimers (with one H-bond), complexes **IVn-Am**, **IVn-Bm**, **Vn-Am**, and **Vn-Bm** (**n, m** = 12 and 16, respectively, except **V12-B12**) possessed the SmCP phase. Furthermore, complexes **Vn-Bm** (**n, m** = 12 and 16, respectively, except **V12-B12**) had the highest transition temperatures and the widest ranges of the SmCP phase.

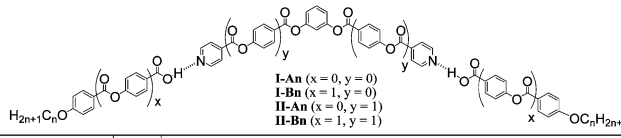
Mesophasic and Thermal Properties of H-Bonded Symmetric Trimers (I-Am, I-Bm, II-Am, and II-Bm with Two H-Bonds). Four series of analogous symmetric trimers (i.e., **I-Am**, **I-Bm**, **II-Am**, and **II-Bm** (**m** = 12 and 16) with five, seven, and nine rings) were investigated for the influence of different ring numbers and H-bonded sites (at the rigid cores) on their mesophasic types and phase transition temperatures, as shown in Table 4 and Figure 3d. Due to the large variation of solubilities in H-donors **Am**, **Bm**, and H-acceptor **II**, phase separation occurred in the preparation of complexes **II-Am** and **II-Bm**, so these complexes could not be compared in this study. Regarding the mesophasic types, a tilt smectic phase was observed in both series of complexes **I-Am** and **I-Bm** (**m** = 12 and 16), in which a SmX phase

TABLE 3: Phase Transition Temperatures and Enthalpies of H-Bonded Seven- and Eight-Ring Asymmetric Heterodimers (with One H-Bond)^a


IVn-Cm ($x = 1, y = 2$)
 Vn-Bm ($x = 2, y = 1$)
 Vn-Cm ($x = 2, y = 2$)

Complex	n	m	Phase transition temperature/°C [Enthalpy/kJ/g]						
IV12-C12	12	12	Phase separation						
IV12-C16	12	16	Phase separation						
IV16-C12	16	12	Phase separation						
IV16-C16	16	16	Phase separation						
V12-B12	12	12	I	152.6 [1.9]	N	142.1 [28.5]	Col _r	107.0 [86.7]	K
V12-B16	12	16	I	156.9 [1.6]	N	148.2 [36.9]	SmCP	110.4 [92.2]	K
V16-B12	16	12	I	158.6 [2.0]	N	149.4 [38.8]	SmCP	101.9 [78.6]	K
V16-B16	16	16	I	155.4 [0.7]	N	152.5 [37.7]	SmCP	114.5 [96.5]	K
V12-C12	12	12	I	156.1 [31.1]	N	133.8 [2.0]	Col _r	92.2 [24.5]	K
V12-C16	12	16	I	159.0 [21.6]	N	147.3 [7.9]	Col _r	119.9 [50.1]	K
V16-C12	16	12	I	159.8 [12.3]	N	138.9 [4.4]	Col _r	104.7 [33.7]	K
V16-C16	16	16	I	158.4 [15.5]	N	147.9 [7.3]	Col _r	111.0 [48.4]	K

^a I = isotropic state; N = nematic phase; Col_r = column rectangular (Col_r) phase; SmCP = polar tilt smectic phase; K = crystalline state. The phase transitions were measured by DSC at the second cooling scan at a cooling rate of 5 °C min⁻¹.

TABLE 4: Phase Transition Temperatures and Enthalpies of H-Bonded Symmetric Trimers (with Two H-Bonds)


I-An ($x = 0, y = 0$)
 I-Bn ($x = 1, y = 0$)
 II-An ($x = 0, y = 1$)
 II-Bn ($x = 1, y = 1$)

Complex	m	Phase transition temperature/°C [Enthalpy/kJ/g]						
I-A12	12	I	108.0 [4.4]	SmC	78.3 [46.8]	K		
I-A16	16	I	113.7 [11.8]	SmC	83.0 [53.3]	K		
I-B12	12	I	168.9 [14.6]	SmC	81.5 [31.9]	SmX	79.8 ^a	K
I-B16	16	I	171.0 [14.1]	SmC	84.3 [29.6]	SmX	76.6 [18.3]	K
II-A12	12	Phase separation						
II-A16	16	Phase separation						
II-B12	12	Phase separation						
II-B16	16	Phase separation						

^a The temperature data is observed in POM only. The phase transitions were measured by DSC at the second cooling scan with a cooling rate of 5 °C min⁻¹. I = isotropic state; SmC = normal tilt smectic phase without polar switching behavior; B1 = column rectangular (Col_r) phase; SmX = undefined smectic phase; K = crystalline state.

was obtained in complexes **I-Bm** with seven rings (at the rigid cores). The mesophasic textures were observed by POM experiments. For instance, complex **I-A12** revealed the tilt smectic phase with spherulite and schlieren textures in Figure 4a, and complex **I-B12** exhibited the tilt smectic (SmC) phase with the fanlike texture in Figure 4b, which were evidence of the tilt smectic (SmC) phase. In addition, complex **I-B12** demonstrated the undefined smectic phase with the arced fanlike texture in Figure 4c.

To compare the phase transition temperatures of symmetric trimers **I-Bm** and **I-Am** ($m = 12$ and 16) (Figure 3c), complexes **I-Bm** (with seven rings) possessed higher isotropization temperatures and wider SmC phase ranges than

complexes **I-Am** (with five rings) due to the longer rigid core of **I-Bm**. Overall, in contrast to H-bonded asymmetric heterodimers (with one H-bond), not all H-bonded symmetric trimers (**I-Am** and **I-Bm** with two H-bonds) show the SmCP phase due to higher flexibilities of two H-bonds in the supramolecular complexes.

IR Characterization. To prove the formation of supramolecules (compared with the transition temperatures of individual components in Figure S1 and Table S1 of the Supporting Information), new transition temperatures and homogeneous phase transitions of H-bonded complexes would be observed in DSC and POM measurements, respectively. In addition, the existence of H-bonds in these H-bonded complexes can be characterized by IR spectra at various temperatures. Therefore, two examples of asymmetric and symmetric H-bonded complexes are demonstrated as follows:

The IR spectra of H-bonded asymmetric complex **V16-B16** (with one H-bond) and its constituents **V16** (H-acceptor) and **B16** (H-donor) are compared in Figure 5 to examine the H-bonds in crystalline and mesophasic states. In contrast to the O-H band of pure **B16** (self-H-bonded dimeric acids) at 2546 cm⁻¹, the weaker O-H bands observed at 2506 and 1920 cm⁻¹ in the H-bonded complex **V16-B16** were indicative of hydrogen bonding between the pyridyl group of H-acceptor **V16** and acidic group of H-donor **B16**. On the other hand, a C=O stretching vibration appeared at 1742 cm⁻¹ in complex **V16-B16**, which showed that the carbonyl group is in a less associated state than that in pure **B16** with a weaker C=O stretching vibration appearing at 1729 cm⁻¹ in either the crystalline phase or mesophases (Figure 5a and b).¹⁹ Both results suggested that H-bonds formed between **B16** and **V16** in both the solid and mesophasic states of complex **V16-B16**.

In addition, similar IR analysis of H-bonds in symmetric H-bonded complex **I-B16** (with one H-bond) was inspected at various temperatures. With the IR evidence of a weak O-H band at 2516 and 1914 cm⁻¹ and less association of C=O stretching vibration at 1740 cm⁻¹, as shown in Figures 5c and d, it revealed the successful supramolecular framework of H-bonded complex **I-B16** by complexation of H-donor **B16** and H-acceptor **I** in 2:1 molar ratio.

Powder XRD Analyses of H-Bonded Asymmetric Heterodimers (with One H-Bond). (i) **Four- and Five-Ring Systems (III_n-Am, III_n-Bm, and IV_n-Am).** The H-bonded molecular organizations of four- and five-ring asymmetric complexes in different mesophases (smectic phases) were investigated by XRD measurements (see Table 5). Wide-angle diffuse peaks corresponding to a *d*-spacing value of 4.6 Å indicated that similar liquidlike, in-plane orders with average intermolecular distances were prevalent inside the smectic layers of all H-bonded complexes. In addition, sharp XRD peaks indexed as (001) were observed at the corresponding *d*-spacing values of *d*₁ = 42.5, 46.1, 46.6, and 49.5 Å in small-angle regions of **III12-A12**, **III12-A16**, **III16-A12**, and **III16-A16**, respectively. The tilt angle values (between the molecular axis and the layer normal) were calculated from the values of *d*-spacing (*d*₁) and molecular length (*L*), where *L* is the theoretical coplanar molecular length from the molecular modeling. Almost equal values of *d*-spacing and calculated *L* were obtained in all complexes **III_n-Am** ($n, m = 12$ and 16), which revealed that LC molecules were nearly perpendicular to the plane surface. Hence, the XRD data supported the existence of the SmA phase, which was also verified by POM experiments to observe the fanlike and homeotropic textures. The analogous XRD results also suggested the SmA phase for

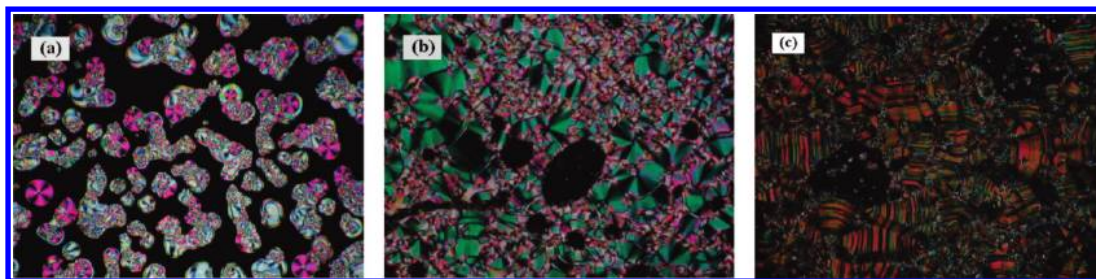


Figure 4. POM textures at the cooling process: (a) the until smectic phase with spherulite and schlieren texture of complex **I-A12** at 100 °C; (b) the till smectic phase with the fanlike texture of complex **I-B12** at 130 °C; (c) the undefined smectic phase with the arced fanlike texture of complex **I-B12** at 80 °C.

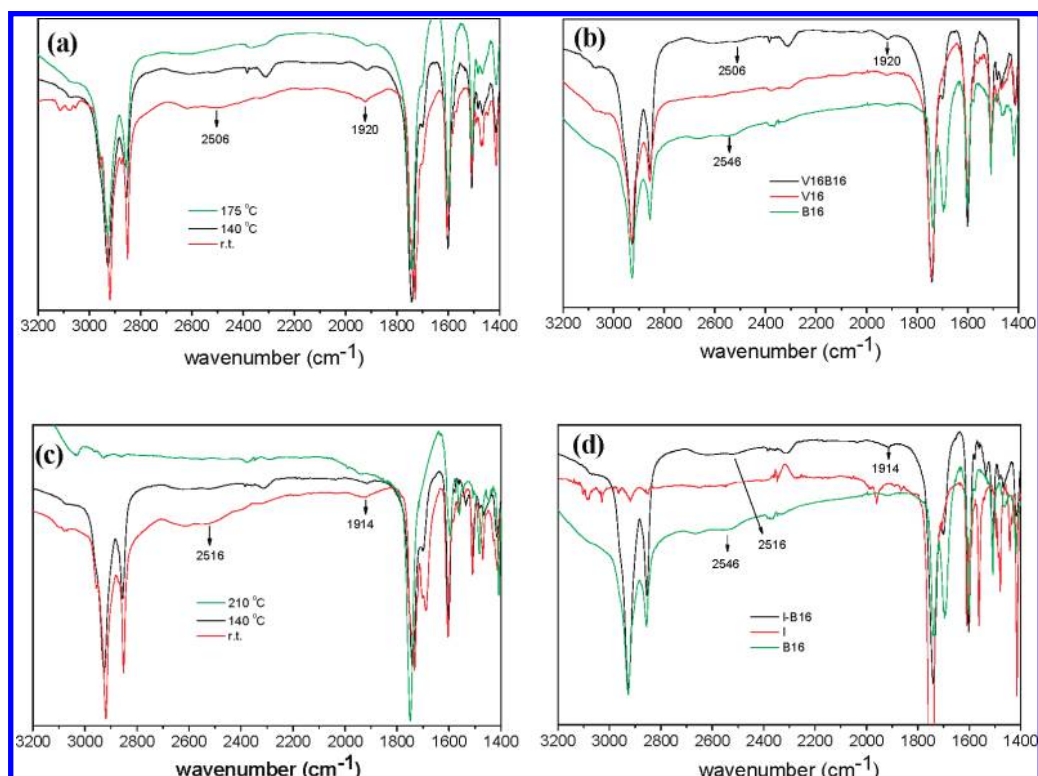


Figure 5. IR spectra of H-bonded asymmetric heterodimeric complex **V16-B16** (a) at variable temperatures and (b) its composed moieties (at room temperature); H-bonded symmetric trimeric complex **I-B16** (c) at variable temperatures and (d) its composed moieties (at room temperature).

TABLE 5: XRD Data of H-Bonded Four- and Five-Ring Asymmetric Hetero-Dimers (with One H-Bond)

complex	measured spacing (d)/Å	Miller index	theoretical length (L)/Å	tilt angle/ $^{\circ}$
III12-A12	42.5	(001)	43.4	11.7
III12-A16	46.1	(001)	46.5	7.5
III16-A12	46.6	(001)	46.7	3.8
III16-A16	49.5	(001)	49.7	5.1
III12-B12	51.9	(001)	52.1	5.9
III12-B16	55.4	(001)	55.6	4.9
III16-B12	54.6	(001)	55.5	10.3
III16-B16	59.2	(001)	59.8	8.2
IV12-A12	42.2	(001)	54.5	39.2
IV12-A16	47.6	(001)	58.3	35.2
IV16-A12	46.3	(001)	58.2	37.2
IV16-A16	50.6	(001)	61.8	35.0

all complexes **III n -B m** , which exhibited a single sharp reflection peak in the small-angle region with d_1 corresponding to the calculated L to prove the SmA phase. The detailed XRD data are illustrated in Table 5.

With respect to complexes **IV n -A m** , sharp peaks indexed as (001) in the small-angle region were obtained at the associated

d -spacing values of $d_1 = 42.2, 47.6, 46.3,$ and 50.6 Å in **IV12-A12, IV12-A16, IV16-A12,** and **IV16-A16**, respectively. The tilt angles (θ) calculated from the values of d_1 and L were around $35-39^{\circ}$, and the tilt angles were normally larger than those of the SmC phase (without polar switching behavior), which has also been confirmed in previous reports.²⁰ It is an indication that tilt lamellar arrangements existed in the mesophasic range of all complexes **IV n -A n** . Therefore, the two-dimensional structures of the SmCP phase in complexes **IV n -A n** were further confirmed by the XRD results.

(ii) Six-Ring Systems (III n -C m , IV n -B m , and V n -A m).

The structural arrangements of six-ring asymmetric complexes **IV n -B m** and **V n -A m** investigated by XRD measurements are shown in Table 6. Only broad peaks of complexes **III n -C m** in small- and wide-angle regions were obtained in the mesophasic ranges, which ruled out the presence of the smectic phase and thus suggested the existence of the nematic phase. However, one set of sharp peaks indexed as (001) with lamellar orders in complexes **IV n -B m** and **V n -A m** were observed at the related d_1 values of $42-52$ Å, which implied the polar smectic (SmCP) phase with tilt angles of $31-42^{\circ}$.

TABLE 6: XRD Data of H-Bonded Six-Ring Asymmetric Hetero-Dimers (with One H-Bond)

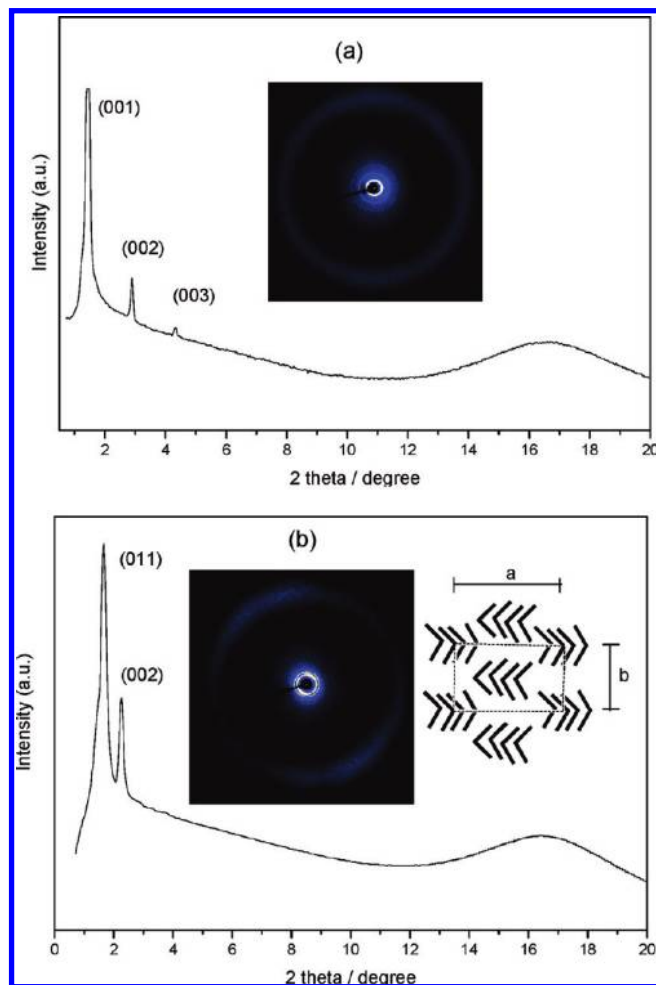
complex	measured spacing (d)/Å	Miller index	theoretical length (L)/Å	tilt angle/ $^\circ$
IV12–B12	42.3	(001)	57.5	42.6
IV12–B16	49.0	(001)	60.9	36.4
IV16–B12	50.3	(001)	60.7	34.1
IV16–B16	52.7	(001)	64.0	34.6
V12–A12	46.6	(001)	54.1	31.0
V12–A16	48.7	(001)	59.2	34.9
	24.4	(002)		
V16–A12	49.0	(001)	59.3	34.3
	24.3	(001)		
V16–A16	51.3	(100)	61.7	33.9

TABLE 7: XRD Data of H-Bonded Seven- and Eight-Ring Asymmetric Heterodimers (with One H-Bond)

complex	measured spacing (d)/Å	Miller index	theoretical length (L)/Å	tilt angle or lattice parameters
V12–B12	44.9	(011)	65.8	$a = 64.8 \text{ \AA}$ $b = 62.3 \text{ \AA}$
	32.4	(002)		
V12–B16	51.3	(001)	69.4	42.3°
	25.8	(002)		
V16–B12	52.4	(001)	$L = 69.6$	41.2°
	26.2	(002)		
V16–B16	54.2	(001)	72.9	41.9°
	27.6	(002)		
V12–C12	17.9	(003)	66.9	$a = 65.2 \text{ \AA}$ $b = 50.6 \text{ \AA}$
	40.0	(011)		
	32.6	(002)		
V12–C16	42.2	(011)	70.5	$a = 65.8 \text{ \AA}$ $b = 55.0 \text{ \AA}$
	32.9	(002)		
V16–C12	41.1	(011)	69.7	$a = 66.2 \text{ \AA}$ $b = 52.4 \text{ \AA}$
	33.1	(002)		
V16–C16	46.3	(011)	73.1	$a = 67.2 \text{ \AA}$ $b = 60.5 \text{ \AA}$
	33.6	(002)		

(iii) *Seven- and Eight-Ring Systems (Vn–Bm and Vn–Cm)*. The structural arrangements of seven- and eight-ring asymmetric complexes **Vn–Bm** and **Vn–Cm** investigated by XRD measurements are shown in Table 7. Regarding the complexes **Vn–Bm**, the tilt smectic arrangements were demonstrated in **V12–B16**, **V16–B12**, and **V16–B16**. For example, sharp layer reflection peaks (up to the third-order diffraction, as shown in Figure 6a) were observed at the associated d -spacing values of $d_1 = 54.2 \text{ \AA}$, $d_2 = 27.6 \text{ \AA}$, and $d_3 = 17.9 \text{ \AA}$, with tilt angles $\sim 42^\circ$ in complex **V16–B16** as the evidence of the tilt lamellar arrangements. However, two sharp reflection peaks indexed as (011) and (002) were observed at the corresponding d -spacing values of $d_1 = 44.9 \text{ \AA}$ and $d_2 = 32.4 \text{ \AA}$ in complex **V12–B12** to reveal the rectangular columnar arrangement.^{5f,21} The analogous XRD results also suggested the Col_r phase for all complexes **Vn–Cm**. For instance, two sharp reflection peaks indexed as (011) and (002) indicated the rectangular columnar arrangement as the example of one- and two-dimensional XRD patterns in complex **V16–C16** (see Figure 6b). The two-dimensional lattice parameters could be calculated as $a = 67.2 \text{ \AA}$ and $b = 60.5 \text{ \AA}$, as shown in the inserted pattern of Figure 5b. All center-rectangular lattices with two-dimensional lattice parameters were identified as a Col_r phase, as revealed in Table 7.

Powder XRD Analyses of H-Bonded Symmetric Trimers (I–Am and I–Bm, with Two H-Bonds). Two series of analogous symmetric trimers with mesomorphic properties (i.e., **I–Am** and **I–Bm** ($m = 12$ and 16) containing 5 and 7 rings) were investigated by XRD measurements to evaluate the influence of different ring numbers (at the rigid cores) on their

**Figure 6.** Powder X-ray diffraction intensity vs angle profiles obtained upon cooling from the isotropic phase: (a) in the polar smectic phase of complex **V16–B16** and (b) in the Col_r phase of complex **V16–C16**.

layer spacing values, as shown in Table 8. The tilt lamellar arrangements with various tilt angles (as shown in Table 8) were confirmed by XRD measurements in the mesophasic ranges of complexes **I–Am** and **I–Bm** ($m = 12$ and 16) according to the observation of sharp and broad diffuse XRD diffraction peaks in small and wide angle regions, respectively. Generally, the tilt angles of complexes **I–Bm** (containing seven rings) are larger than those of complexes **I–Am** (containing five rings).

Spontaneous Polarization (P_s) Behavior and Dielectric Analysis of H-Bonded Complexes. To prove the polar switching properties in symmetric trimer and asymmetric heterodimer complexes, the triangular wave method²² was applied to measure the switching current behavior (i.e., the spontaneous polarization) under $4.25\text{-}\mu\text{m}$ -thick parallel rubbing cells. Two current peaks per half period of an applied triangular voltage were obtained in the switching current response curves of all SmCP phase in the asymmetric heterodimeric complexes **IVn–Am**,

TABLE 8: XRD Data of H-Bonded Symmetric Trimers (with Two H-Bonds)

complex	measured spacing (d)/Å	Miller index	theoretical length (L)/Å	tilt angle/ $^\circ$
I–A12	32.5	(001)	46.2	45.3
I–A16	40.9	(001)	50.9	36.5
I–B12	33.5	(001)	61.1	56.7
I–B16	37.6	(001)	66.6	55.6

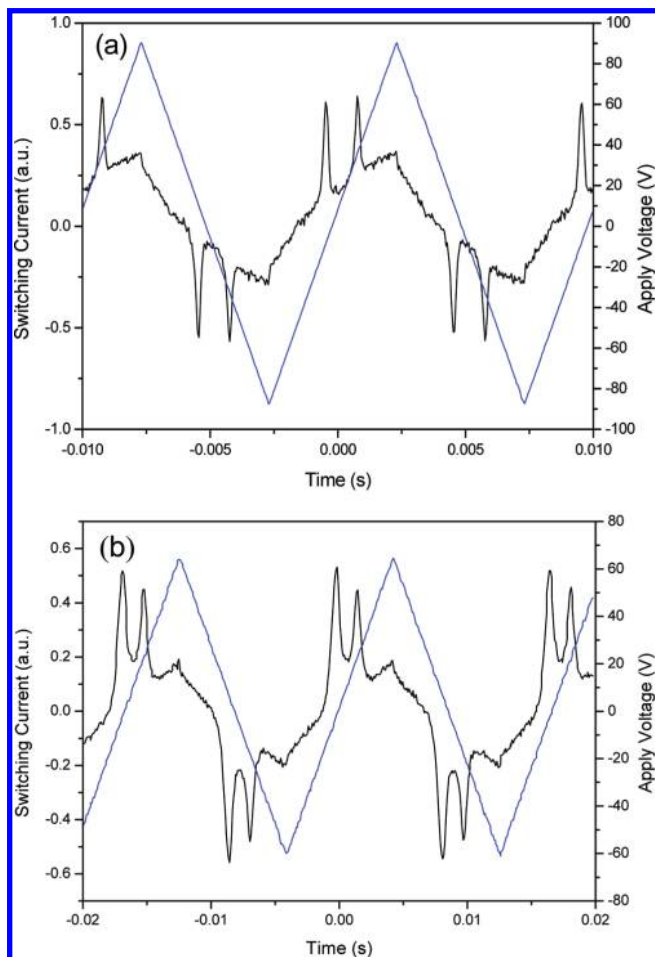


Figure 7. Switching current responses of H-bonded asymmetric heterodimers (a) **IV12-A12** at 95 °C (as $V_{pp} = 180$ V, $f = 60$ Hz) and (b) **V16-B16** at 130 °C (as $V_{pp} = 120$ V and $f = 100$ Hz) by applying a triangular wave (in parallel rubbing cells with 4.25 μm thickness).

IVn-Bm, **Vn-Am**, and **Vn-Bm** (n and $m = 12$ and 16 , except **V12-B12**). For instance, the two-peak switching current response curves of complexes **IV12-A12** and **V16-B16** are shown in Figure 7. Here, the characteristic behavior of a sequential electric response was due to a ferroelectric state switched into an antiferroelectric ground state and back to the opposite ferroelectric state, which confirmed the SmCP_A ($A = \text{antiferroelectric behavior}$) structure of the B2 phase in these asymmetric heterodimeric complexes.²³ The P_s values (the saturated values at high voltages) could be calculated in the ranges of 200–240, 135–140, 140–145, and 115–125 nC/cm^2 for complexes **Vn-Bn**, **Vn-An**, **IVn-Bn**, and **IVn-An**, respectively. The P_s values were higher in complexes with longer rigid-core rings but were not influenced by the H-bonded sites and flexible chain lengths. As shown in Figure 8, the spontaneous polarization values vs applied electric fields were surveyed in the SmCP phase of the H-bonded asymmetric heterodimers (**Vn-Bn**, **Vn-An**, **IVn-Bn**, and **IVn-An**), where the maximum applied voltages (peak to peak) were $V_{pp} = 600$ – 650 V and the saturated P_s values were reached at voltages above $V_{pp} = 200$ – 230 V. In contrast, the saturated P_s value of 500 nC/cm^2 in compound **S12** was obtained at a much higher voltage above $V_{pp} = 320$ V in our study (as shown in Figure S2 of the Supporting Information). Hence, the H-bonded substitution for the covalently bonded ester groups in the bent-core systems would not only decrease the phase transition temperatures but also reduce the voltages of the saturated P_s values due to the softer rigid-core configurations in the H-bonded complexes.

However, since the B1_{rev} and $\text{B1}_{\text{rev,tilt}}$ phases have the switching phenomena by applying electric fields,^{10a,24} the Col_l (B1) phase in complexes **V12-B12** and **Vn-Cm** ($n, m = 12$ and 16) was confirmed considering no switching current behavior was observed. Moreover, the Col_l phase was further verified in view of no texture variation (in 4.25- μm -thick parallel rubbing cells) under polarizing optical microscopy by applying

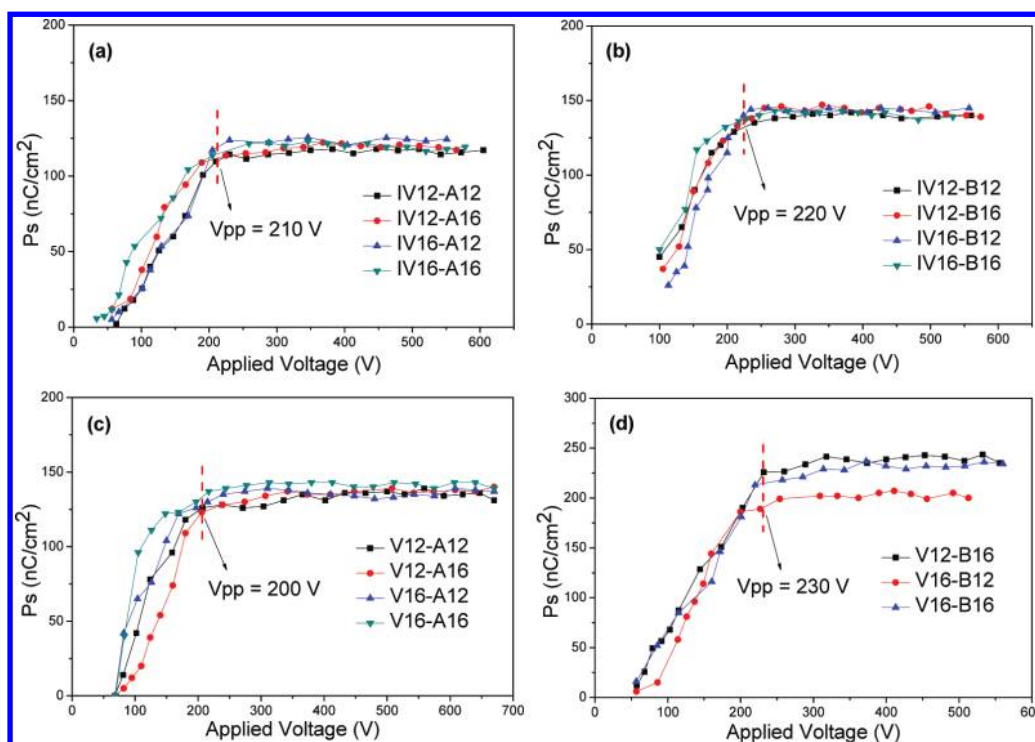


Figure 8. P_s values as a function of applied voltages (at the SmCP phase as $f = 60$ Hz) for complexes (a) **IVn-Am**, (b) **IVn-Bm**, (c) **Vn-Am**, and (d) **Vn-Bm**.

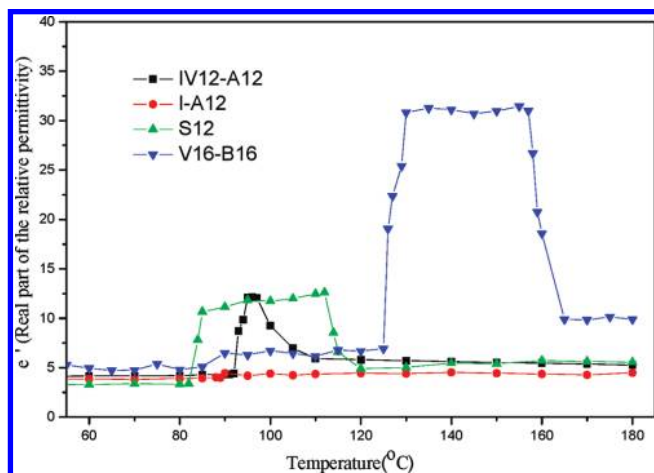


Figure 9. Dielectric permittivity studies of compound **S12** and H-bonded complexes **IV12-A12**, **I-A12**, and **V16-B16** in the cooling processes.

electric fields up to 400 V_{pp} (peak to peak). Regarding the electrooptical properties of the SmC phase in symmetric trimers **I-Am** and **I-Bm** ($m = 12$ and 16 , with two H-bonds), it was proven that no switching current responses were observed under AC fields. As the applied electric field was raised to 200 V_{pp}, the fanlike domain was broken into the grainy domain, which suggested the unstable H-bonds were due to the symmetric bent-core structures with two H-bonds.

The antiferroelectricity was also further evidenced by the dielectric permittivity studies, and compound **S12** and H-bonded complexes **IV12-A12**, **V16-B16**, and **I-A12** were investigated under their cooling processes at a frequency of 5 kHz in nonrubbing cells (9 μm cell gap), as shown in Figure 9. Higher permittivity values ($\epsilon \sim 32$) of the SmCP phase were observed than those of the isotropic, nematic, and crystalline states in complex **V16-B16**, which indicates the antiferroelectric polar smectic phase.²⁵ Similar higher permittivity values ($\epsilon \sim 10$ – 15) of the SmCP phase in compound **S12** and H-bonded complex **IV12-A12** were also obtained. However, no higher permittivity values were achieved in the SmC phase of complex **I-A12** to further prove the tilt smectic phase without polar switching behavior.

Chirality Investigation. In addition to the triangular wave method, a switching process could also be checked through the rotation of the extinction crosses (Figure 10) by applying (or after removing) opposite dc electric fields in the bent-core H-bonded complexes with the SmCP phase. For instance, circular domains of complex **IV16-A16** were formed in the SmCP mesophasic range, in which the smectic layers were circularly arranged around the centers of the domains. The layer structures were arranged according to the domain models proposed by Link et al.²⁶ As shown in Figure 10, the rotation of the extinction crosses during the switched on and off states in complexes **IV16-A16** and **V16-B16** demonstrated the chiral domain behavior.²⁷ In view of Figure 10a and c, by applying dc electric fields (with reverse polarities), the extinction crosses rotated either counterclockwise or clockwise (i.e., rotated oppositely with positive and negative fields), indicating a synclinal tilt in the ferroelectric state (SmC_SP_F). By removing the electric fields (off state), the extinction crosses were reoriented back to the crossed polarizer directions (see Figure 10b), indicating an anticlinal tilt in the antiferroelectric ground state (SmC_AP_A). Similarly, complex **V16-B16** yielded the synclinal and ferroelectric SmC_SP_F state by applying opposite

dc electric fields (see Figure 10d and f), and the SmC_AP_A state after removing electric fields (see Figure 10e).

The chiral domain behavior could also be proven by the method of rotating the polarizer without applying electric fields.¹⁵ For example, the polarizer was rotated clockwise by a small angle of 10° from the crossed position in complex **V16-B16**, then the dark and bright domains become clearly distinguishable (see Figure 11a). On rotating the polarizer counterclockwise by the same angle (10°) from the crossed position, the previously observed dark domains turned to bright domains, and vice versa (see Figure 11b). This observation was also indicative of the occurrence of chiral domains with opposite handedness.

Theoretical Analyses of Dipole Moments and Bent Angles in H-Bonded Complexes. To analyze the variation of the polarities by insertion of single and double H-bonds in H-bonded complexes, the supramolecular dipole moments, electron cloud distributions, and bend angles were calculated by molecular modeling, which would influence the polar switching behavior in covalently and H-bonded bent-core structures with suitable bent cores and flexible chains. Four simplified bent-core structures, including H-bonded complexes **I-A1**, **III1-B1**, and **IV1-A1** and covalently bonded compound **S1**, bearing methoxy groups at their terminuses were designed as shown in Figure 12, where the electron cloud distributions of these model structures are demonstrated. Due to the H-bonds, the polarities and dipoles of complexes **I-A1**, **III1-B1**, and **IV1-A1** were reduced by the noncovalent aggregation of H-bonded electrons at benzoic acid positions. As shown in Table 9, the theoretical calculations of molecular modeling for covalently and H-bonded bent-core structures with lowest energies (see Supporting Information) were simulated by Gaussian0315 at the B3LYP level with the 6-31G(d) basis set. Regarding covalently bonded compound **S1**, the projected low values of dipole moments along the X and Z directions were equal to 1.394 and 0.172 D, which were mutually offset due to the symmetric structure. However, a large value of -4.123 D in the Y direction was evaluated to contribute to the total dipole moment in the molecular polar direction. Because of the symmetric skeleton in H-bonded complex **I-A1**, similar results of the projected low values of dipole moments in the X and Z dimensions were eliminated to 1.041 and -0.090 D, and a very small value of 1.126 D was acquired in the Y dimension due to the noncovalent electron aggregation of H-bonded sites. Hence, a much smaller total dipole moment of 1.53 D (along with the smallest polarity) was obtained for the simplified H-bonded complex **I-A1**, thus suggesting the nonpolar switching behavior for H-bonded symmetric trimers **I-Am** (with two H-bonds). In contrast to complex **I-A1**, the polar destruction was also obtained in the Y direction (-2.971 D) for complex **IV1-A1** due to the noncovalent electron aggregation of H-bonded sites. However, the projective dipole contribution along X and Z directions (-3.418 and -0.022 D, respectively) were revealed as a result of the asymmetric structure in complex **IV1-A1**. Therefore, the total dipole moment of 4.53 D in complex **IV1-A1** was achieved to suggest the polar switching behavior for H-bonded asymmetric dimers **IVn-Am** (with one H-bond). Comparing complexes **I-A1** and **IV1-A1**, the polar switching behavior of H-bonded asymmetric dimers **IVn-Am** can be expected according to the visualization of the simplified model complex **IV1-A1** with larger total dipole moments.

In the investigation of bend angle effect on the polar switching behavior of bent-core liquid crystals, the suitable bend angle for bent-core molecular configuration is better close to 120°

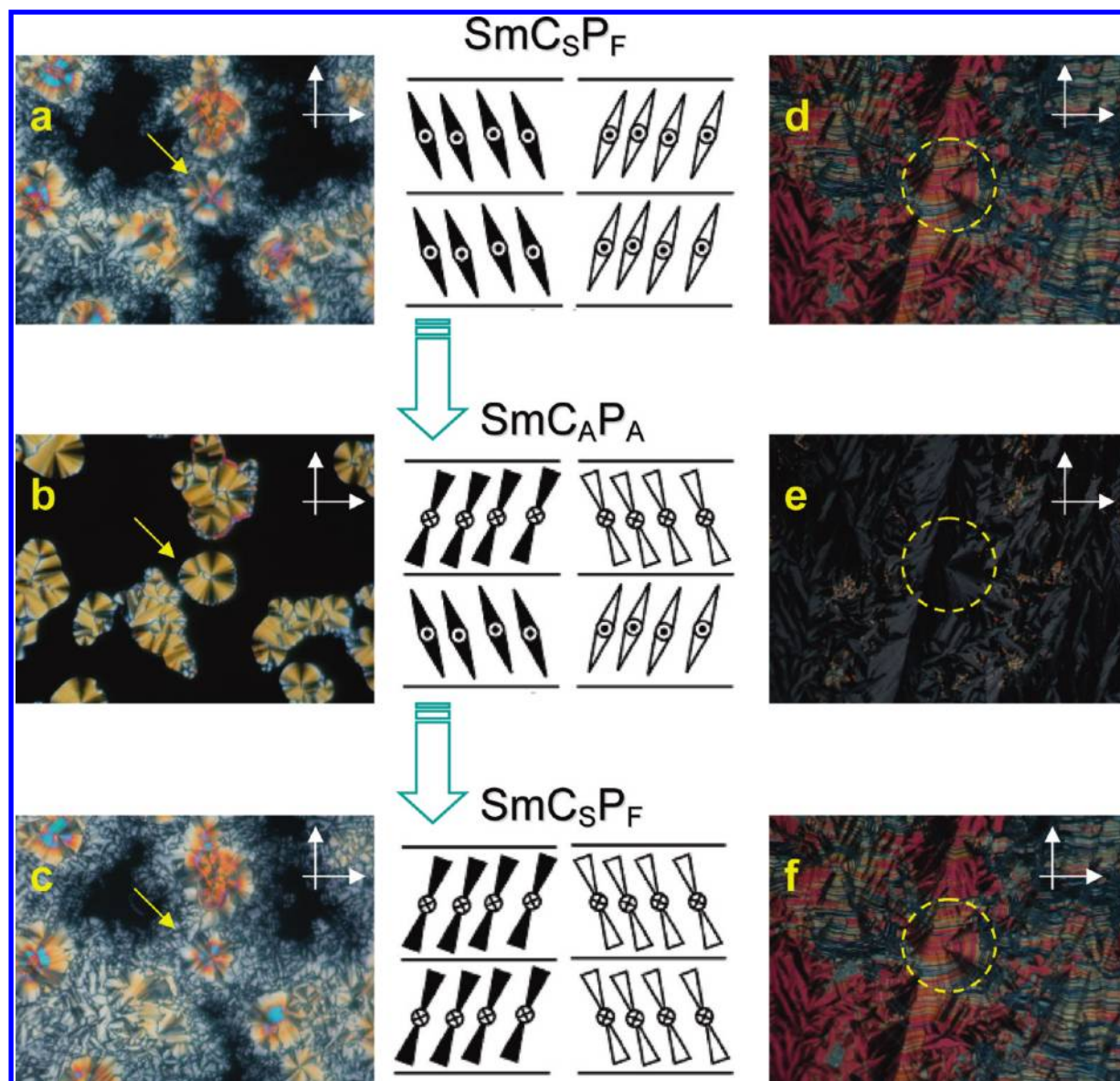


Figure 10. POM textures of the antiferroelectric $\text{SmC}_{\text{A}}\text{P}_{\text{A}}$ chiral domain (in a parallel rubbing cell with a cell gap of $4.25\ \mu\text{m}$) in five-ring complex **IV16–A16** by applying dc electric fields from (a) -50 to (b) 0 to (c) $+50$ V; in seven-ring complex **V16–B16** by applying dc electric fields from (d) -50 to (e) 0 to (f) $+50$ V. (White arrows are the directions of polarizers and analyzers.)

(or in the range of 110 – 130°).^{28,5f} Usually, calamitic LC materials possessing bent-core configurations with bend angles larger than 130° or less than 110° will reveal normal mesophases without polar switching behavior, such as the smectic C, smectic A, and nematic phases. In our theoretical molecular modeling, bend angles of almost 120° and 114° were obtained in molecules **S1** and **IV1–A1**, respectively, to support the existence of spontaneous polarization. However, the lower bend angle values (less than $\sim 100^\circ$) were achieved in complex **III1–B1** due to the near central-site H-bonds, even if the sufficient total dipole moment values (~ 4.10 D) were acquired. It would be speculated that the deficiency of polar switching behavior in H-bonded asymmetric dimers with single near-central H-bonded sites, such as complexes **III n –B m** and **III n –C m** , was a result of their small bend angles (less than $\sim 100^\circ$). Overall, the asymmetric H-bonded molecular design as well as the suitable molecular bend angle is useful to enhance the total dipole moments and polarities in accordance with the theoretical analyses of molecular modeling, and the spontaneous polarization and switching behavior can be not only experimentally proven but also theoretically predicted in our study.

Conclusions

In summary, several series of novel banana-shaped liquid crystalline supramolecules consisting of H-bonded symmetric trimers (with two H-bonds) and asymmetric heterodimers (with one H-bond) were self-assembled by appropriate molar ratios of proton donors and acceptors. The influences of H-bonded linking positions and aromatic ring numbers (in the rigid cores) as well as the chain lengths (in the flexible parts) on the mesomorphism and the switching behavior of the bent-core supramolecules were reported. Moreover, the voltage-dependent switching properties of spontaneous polarization (P_s) in the polar smectic C phase of the banana-shaped H-bonded complexes were observed. In the normal field-off state, except for the supramolecular structures with longer rigid cores or shorter flexible chains possessing the rectangular columnar (Col_r or B1) phase, the $\text{SmC}_{\text{A}}\text{P}_{\text{A}}$ phase was revealed in most supramolecular asymmetric heterodimers (with one H-bond), which was switched to the $\text{SmC}_{\text{S}}\text{P}_{\text{F}}$ phase by applying electric fields. In addition, the SmA and nematic phases were observed in H-bonded

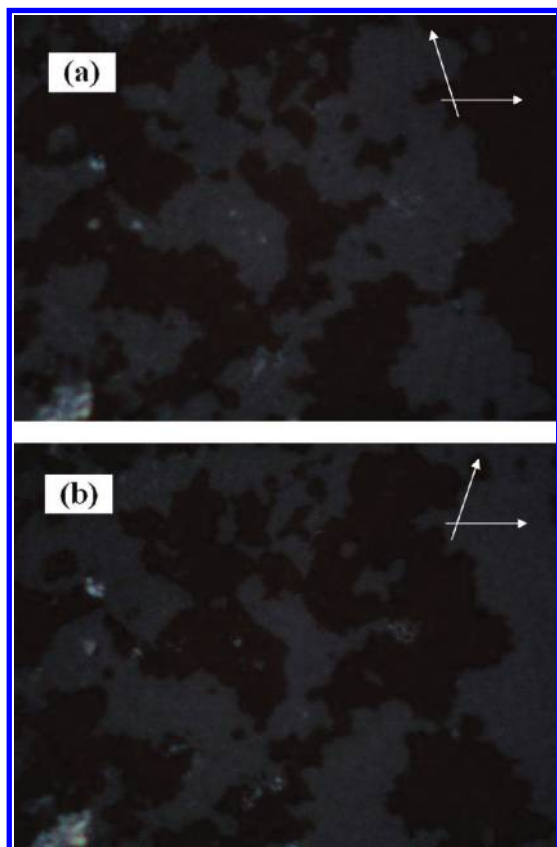


Figure 11. Chiral domain textures for complex **V16-B16**. (Arrows are the directions of polarizers and analyzers.)

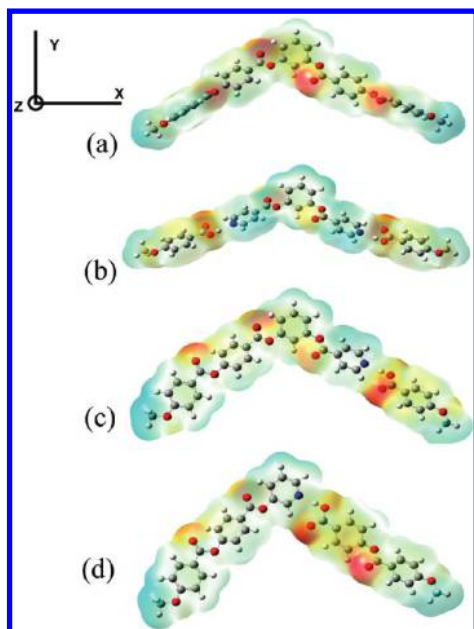


Figure 12. Molecular electrostatic potential mapped on the electron density isosurface of 0.0004 au of the lowest energy structure for the four bent-core structures: (a) **S1**, (b) **I-A1**, (c) **IV1-A1**, and (d) **III1-B1**.

asymmetric dimers with H-bonded sites close to the core center, but the polar smectic C phase dominated for those with H-bonded sites apart from the core center. Compared with the fully covalently bonded analogue, lower transition temperatures and lower threshold voltages were developed in H-bonded asymmetric dimers with the polar smectic C phase. The existence of polar switching behavior in the polar

TABLE 9: Calculated Dipole Moments and Bent Angles of Optimized Covalently and H-Bonded Bent-Core Structures at the B3LYP/6-31G(d) Level

compound	bend angle ($^{\circ}$) ^a	axial	dipole moment (Debye)
S1	120.0	X	1.394
		Y	-4.123
		Z	0.172
		total	4.35
I-A1	131.2	X	1.041
		Y	1.126
		Z	-0.090
		total	1.53
IV1-A1	113.7	X	-3.418
		Y	-2.971
		Z	-0.022
		total	4.53
III1-B1	99.6	X	-1.385
		Y	-3.837
		Z	-0.457
		total	4.10

^a Bend angle ($^{\circ}$) measured as the angle between the first, central, and final benzene rings' centers of the bent-core structures. The dipole moments of the lowest energy structure are given, and the calculated dipoles are in the range of 4.00–8.85 (**S1**), 0.21–1.94 (**I-A1**), 4.53–6.69 (**IV1-A1**), and 4.10–7.24 (**III1-B1**) (see Supporting Information). Sets of unique conformations within 1 kcal/mol of the global minimum from conformational search using molecular mechanics force-field were used for full geometry optimization at the B3LYP/6-31G(d) level.

smectic C phase of asymmetric heterodimers (with one H-bond) related to the molecular configurations with higher dipole moments as well as the suitable bend angle was further demonstrated by the theoretical calculations of molecular modeling. In addition, the lack of polar switching behavior in supramolecular symmetric trimers (with two H-bonds), which exhibited the regular SmC phase with weak electrical stabilities, might be related to their configurations with smaller dipole moments. Finally, due to the low electrical stabilities of the H-bonded symmetric trimers (with two H-bonds), their supramolecular architectures with the polar smectic C phase may be preserved or created by the stabilization H-bonded structures through further auxiliary techniques (such as copolymerization and blending with covalently bonded analogues) in the future studies. Finally, the spontaneous polarization and switching behavior of H-bonded banana-shaped LC materials are for the first time experimentally proven and theoretically predicted in our study.

Acknowledgment. We are thankful for the financial support from the National Science Council of Taiwan (ROC) through NSC 96-2113-M-009-015. We are also grateful to the National Center for High-performance Computing for computer time and facilities. The powder XRD measurements were supplied by beamline BL17A (charged by Dr. Jey-Jau Lee) of the National Synchrotron Radiation Research Center (NSRRC) in Taiwan.

Supporting Information Available: The detailed synthetic procedures, schemes, thermal properties, and phase transitions of all H-donors and H-acceptors; Ps values of compound **S12** at various voltages; figures and tables for low-energy structures of compounds **S1**, **I-A1**, **IV1-A1**, and **III1-B1**

by theoretical calculations of molecular modeling. This information is available free of charge via the Internet at <http://pubs.acs.org>.

References and Notes

- (1) (a) Ikkala, O.; Brinke, G. T. *Science* **2002**, *295*, 2407. (b) Stupp, S. I.; Son, S.; Lin, H. C.; Li, L. S. *Science* **1993**, *259*, 59. (c) Kato, T.; Mizoshita, N.; Kishimoto, K. *Angew. Chem., Int. Ed.* **2006**, *45*, 38. (d) Kumar, U. J.; Frechet, M. J.; Kato, T.; Ujije, S.; Imura, K. *Angew. Chem., Int. Ed.* **1992**, *31*, 1531. (e) Tsonchev, S.; Niece, K. L.; Schatz, G. C.; Ratner, M. A.; Stupp, S. I. *J. Phys. Chem. B* **2008**, *112*, 441. (f) Velichko, Y. R.; Stupp, S. I.; de la Cruz, M. O. *J. Phys. Chem. B* **2008**, *112*, 2326.
- (2) (a) Hofmeier, H.; Schubert, U. S. *Chem. Commun.* **2005**, 2423. (b) Pollino, J. M.; Weck, M. *Chem. Soc. Rev.* **2005**, *34*, 193. (c) Moulton, B.; Zaworotko, M. J. *Chem. Rev.* **2001**, *101*, 1629. (d) Kato, T.; Matsuoka, T.; Nishii, M.; Kamikawa, Y.; Kanie, K.; Nishimura, T.; Yashima, E.; Ujije, S. *Angew. Chem., Int. Ed.* **2004**, *43*, 1969.
- (3) (a) Nakata, M.; Shao, R. F.; MacLennan, J. E.; Weissflog, W.; Clark, N. A. *Phys. Rev. Lett.* **2006**, *96*, 067802. (b) Rickard, M.; Nakata, M.; Takezoe, H.; Watanabe, J.; Clark, N. A. *Phys. Rev. Lett.* **2005**, *87*, 261115. (c) Meyer, R. B.; Liebert, L.; Strzelecki, L.; Keller, P. *J. Phys. (Paris) Lett.* **1975**, *36*, 69. (d) Chandani, A. D. L.; Ouchi, Y.; Takezoe, H.; Fukuda, A.; Terashima, K.; Furukawa, K.; Kishi, A. *Jpn. J. Appl. Phys.* **1989**, *28*, 1261. (e) Fukuda, A.; Takanishi, Y.; Isokaki, T.; Ishikawa, K.; Takezoe, H. *J. Mater. Chem.* **1994**, *4*, 997.
- (4) (a) Niori, T.; Sekine, F.; Watanabe, J.; Furukawa, T.; Takezoe, H. *J. Mater. Chem.* **1996**, *6*, 1231. (b) Sekine, T.; Niori, T.; Watanabe, J.; Furukawa, T.; Choi, S. W.; Takezoe, H. *J. Mater. Chem.* **1997**, *7*, 1307.
- (5) (a) Kang, S.; Saito, Y.; Watanabe, N.; Tokita, M.; Takanishi, Y.; Takezoe, H.; Watanabe, J. *J. Phys. Chem. B* **2006**, *110*, 5205. (b) Lee, S. K.; Shi, L.; Tokita, M.; Takezoe, H.; Watanabe, J. *J. Phys. Chem. B* **2007**, *111*, 8698. (c) Lee, S. K.; Shi, L.; Tokita, M.; Watanabe, J. *J. Phys. Chem. B* **2008**, *112*, 6762. (d) Pocięcha, D.; Ohta, K.; Januszko, A.; Kaszynski, P.; Endo, Y. *J. Mater. Chem.* **2008**, *18*, 2978. (e) Lee, S. K.; Heo, S.; Lee, J. G.; Kang, K. T.; Kumazawa, K.; Nishida, K.; Shimbo, Y.; Takanishi, Y.; Watanabe, J.; Doi, T.; Takahashi, T.; Takazoe, H. *J. Am. Chem. Soc.* **2005**, *127*, 11085. (f) Pelzl, G.; Diele, S.; Weissflog, W. *Adv. Mater.* **1999**, *11*, 707. (g) Reddy, R. A.; Dantlgraber, G.; Baumeister, U.; Tschierske, C. *Angew. Chem., Int. Ed.* **2006**, *45*, 1. (h) Dantlgraber, G.; Shen, D.; Diele, S.; Tschierske, C. *Chem. Mater.* **2002**, *14*, 1149. (i) Reddy, R. A.; Sadashiva, B. K. *J. Mater. Chem.* **2004**, *14*, 1936. (j) Dunemann, U. M.; Schroder, W.; Reddy, R. A.; Pelzl, G.; Diele, S.; Weissflog, W. *J. Mater. Chem.* **2005**, *15*, 4051. (k) Keith, C.; Reddy, R. A.; Hahn, H.; Lang, H.; Tschierske, C. *Chem. Commun.* **2004**, 1898. (l) Reddy, R. A.; Sadashiva, B. K.; Raghunathan, V. A. *Chem. Mater.* **2004**, *16*, 4050. (m) Keith, C.; Dantlgraber, G.; Reddy, R. A.; Baumeister, U.; Tschierske, C. *Chem. Mater.* **2007**, *19*, 694. (n) Yang, P. J.; Lin, H. C. *Liq. Cryst.* **2006**, *33*, 587.
- (6) (a) Yelamaggad, C. V.; Shashikala, I. S.; Li, Q. *Chem. Mater.* **2007**, *19*, 6561. (b) Kumar, P.; Hiremath, U. S.; Yelamaggad, C. V.; Rossberg, A. G.; Krishnamurthy, K. S. *J. Phys. Chem. B* **2008**, *112*, 9270. (c) Kumar, P.; Marinov, Y. G.; Hinov, H. P.; Hiremath, U. S.; Yelamaggad, C. V.; Krishnamurthy, K. S.; Petrov, A. G. *J. Phys. Chem. B* **2009**, *113*, 9168.
- (7) (a) Keith, C.; Reddy, R. A.; Baumeister, U.; Hahn, H.; Lang, H.; Tschierske, C. *J. Mater. Chem.* **2006**, *16*, 3444. (b) Keith, C.; Reddy, R. A.; Hahn, H.; Lang, H.; Tschierske, C. *Chem. Commun.* **2004**, 1898. (c) Dantlgraber, G.; Eremin, A.; Diele, S.; Hauser, A.; Kresse, H.; Pelzl, G.; Tschierske, C. *Angew. Chem., Int. Ed.* **2002**, *41*, 2408. (d) Reddy, R. A.; Baumeister, U.; Keith, C.; Tschierske, C. *J. Mater. Chem.* **2007**, *17*, 62.
- (8) (a) Keith, C.; Reddy, R. A.; Tschierske, C. *Chem. Commun.* **2005**, 871. (b) Barbera, J.; Gimeno, N.; Monreal, L.; Pinol, R.; Ros, M. B.; Serrano, J. L. *J. Am. Chem. Soc.* **2004**, *126*, 7190. (c) Choi, E. J.; Ahn, J. C.; Chien, L. C.; Lee, C. K.; Zin, W. C.; Kim, D. C.; Shin, S. T. *Macromolecules* **2004**, *37*, 7. (d) Chen, X.; Tenneti, K. K.; Li, C. Y.; Bai, Y.; Wan, X.; Fan, X.; Zhou, Q.-F.; Rong, L.; Hsiao, B. S. *Macromolecules* **2007**, *40*, 840.
- (9) (a) Dantlgraber, G.; Diele, S.; Tschierske, C. *Chem. Commun.* **2002**, 2768. (b) Kosata, B.; Tamba, G. M.; Baumeister, U.; Pelzl, G.; Diele, S.; Pelzl, G.; Galli, G.; Samaritani, S.; Agina, E. V.; Boiko, N. I.; Shibaev, V. P.; Weissflog, W. *Chem. Mater.* **2006**, *18*, 691. (c) Sepelj, M.; Lesac, A.; Baumeister, U.; Diele, S.; Bruce, D. W.; Hamersak, Z. *Chem. Mater.* **2006**, *18*, 2050. (d) Keith, C.; Reddy, R. A.; Baumeister, U.; Hahn, H.; Lang, H.; Tschierske, C. *J. Mater. Chem.* **2006**, *16*, 3444. (e) Umadevi, S.; Sadashiva, B. K.; Murthy, H. N. S.; Raghunathan, V. A. *Soft Matter* **2006**, *2*, 210. (f) Tamba, M.; Kosata, G. B.; Pelzl, G.; Diele, S.; Pelzl, G.; Vakhovskaya, Z.; Kresse, H.; Weissflog, W. *Soft Matter* **2006**, *2*, 60.
- (10) (a) Kardas, D.; Prehm, M.; Baumeister, U.; Pocięcha, D.; Reddy, R. A.; Mehl, G. H.; Tschierske, C. *J. Mater. Chem.* **2005**, *15*, 1722. (b) Dantlgraber, G.; Baumeister, U.; Diele, S.; Kresse, H.; Luhmann, B.; Lang, H.; Tschierske, C. *J. Am. Chem. Soc.* **2002**, *124*, 14852.
- (11) (a) Ros, M. B.; Serrano, J. L.; de la Fuente, M. R.; Folia, C. L. *J. Mater. Chem.* **2005**, *15*, 5093. (b) Reddy, R. A.; Tschierske, C. *J. Mater. Chem.* **2006**, *16*, 907.
- (12) Martin, P. J.; Bruce, D. W. *Liq. Cryst.* **2007**, *6*, 767.
- (13) (a) Gimeno, N.; Ros, M. B.; Serrano, J. L.; de la Fuente, M. R. *Angew. Chem., Int. Ed.* **2004**, *43*, 5235. (b) Barbera, J.; Gimeno, N.; Pintre, I.; Ros, M. B.; Serrano, J. L. *Chem. Commun.* **2006**, 1212. (c) Gimeno, N.; Ros, M. B.; Serrano, J. L. *Chem. Mater.* **2008**, *20*, 1262. (d) Perez, A.; Gimeno, N.; Vera, F.; Ros, M. B.; Serrano, J. L.; de la Fuente, M. R. *Eur. J. Org. Chem.* **2008**, 826.
- (14) (a) Mohamandi, F.; Richards, N. G. J.; Guida, W. C.; Liskamp, R.; Lipton, M.; Caulfield, C.; Chang, G.; Hendrickson, T.; Still, W. C. *J. Comput. Chem.* **1990**, *11*, 400. (b) Weiner, S. J.; Kollman, P. A.; Case, D. A.; Singh, U. C.; Chio, C.; Alagona, G.; Profeta, S.; Weiner, P. *J. Am. Chem. Soc.* **1984**, *106*, 765. (c) Weiner, S. J.; Kollman, P. A.; Case, D. A. *J. Comput. Chem.* **1986**, *7*, 230. (d) Still, W. C.; Tempczyk, A.; Hawley, R. C.; Hendrickson, T. *J. Am. Chem. Soc.* **1990**, *112*, 6127.
- (15) Frisch, M. J.; Trucks, G. W.; Schlegel, H. B.; Scuseria, G. E.; Robb, M. A.; Cheeseman, J. R.; Montgomery, J. A.; Vreven, T., Jr.; Kudin, K. N.; Burant, J. C.; Millam, J. M.; Iyengar, S. S.; Tomasi, J.; Barone, V.; Mennucci, B.; Cossi, M.; Scalmani, G.; Rega, N.; Petersson, G. A.; Nakatsuji, H.; Hada, M.; Ehara, M.; Toyota, K.; Fukuda, R.; Hasegawa, J.; Ishida, M.; Nakajima, T.; Honda, Y.; Kitao, O.; Nakai, H.; Klene, M.; Li, X.; Knox, J. E.; Hratchian, H. P.; Cross, J. B.; Bakken, V.; Adamo, C.; Jaramillo, J.; Gomperts, R.; Stratmann, R. E.; Yazyev, O.; Austin, A. J.; Cammi, R.; Pomelli, C.; Ochterski, J. W.; Ayala, P. Y.; Morokuma, K.; Voth, G. A.; Salvador, P.; Dannenberg, J. J.; Zakrzewski, V. G.; Dapprich, S.; Daniels, A. D.; Strain, M. C.; Farkas, O.; Malick, D. K.; Rabuck, A. D.; Raghavachari, K.; Foresman, J. B.; Ortiz, J. V.; Cui, Q.; Baboul, A. G.; Clifford, S.; Cioslowski, J.; Stefanov, B. B.; Liu, G.; Liashenko, A.; Piskorz, P.; Komaromi, I.; Martin, R. L.; Fox, D. J.; Keith, T.; Al-Laham, M. A.; Peng, C. Y.; Nanayakkara, A.; Challacombe, M.; Gill, P. M. W.; Johnson, B.; Chen, W.; Wong, M. W.; Gonzalez, C.; Pople, J. A. *Gaussian 03, Revision D.02*; Gaussian, Inc.: Wallingford CT, 2004.
- (16) Cativiela, C.; Serrano, J. L.; Zurbano, M. M. *J. Org. Chem.* **1995**, *60*, 3074.
- (17) (a) Schroder, M. W.; Diele, S.; Pelzl, G.; Weissflog, W. *Chem. Phys. Chem.* **2004**, *5*, 99. (b) Pelzl, G.; Diele, S.; Weissflog, W. *Adv. Mater.* **1999**, *11*, 707.
- (18) (a) Sekine, T.; Niori, T.; Sone, M.; Watanabe, J.; Choi, S. W.; Takanishi, Y.; Takezoe, H. *Jpn. J. Appl. Phys.* **1997**, *36*, 6455. (b) Dehne, H.; Potter, M.; Sokolowski, S.; Weissflog, W.; Diele, S.; Pelzl, G.; Wirth, I.; Kresse, H.; Schmalz, H.; Grande, S. *Liq. Cryst.* **2001**, *28*, 1269. (c) Reddy, R. A.; Sadashiva, B. K. *Liq. Cryst.* **2003**, *30*, 1031.
- (19) (a) Wu, C. W.; Lin, H. C. *Macromolecules* **2006**, *39*, 7985. (b) Lin, H. C.; Sheu, H. Y.; Chang, C. L.; Tsai, C. *J. Mater. Chem.* **2001**, *11*, 2958.
- (20) (a) Prasad, V.; Kang, S. W.; Kumar, S. *J. Mater. Chem.* **2003**, *13*, 1259. (b) Murthy, H. N. S.; Sadashiva, B. K. *Liq. Cryst.* **2004**, *31*, 1337.
- (21) Shen, D.; Diele, S.; Pelzl, G.; Wirth, I.; Tschierske, C. *J. Mater. Chem.* **1999**, *9*, 661.
- (22) Miyasato, K.; Abe, S.; Takazoe, H.; Fukuda, A.; Kuze, E. *Jpn. J. Appl. Phys.* **1983**, *22*, 661.
- (23) Zenyoyi, M.; Takanishi, Y.; Ishikawa, K.; Thisayukta, J.; Watanabe, J.; Takezoe, H. *J. Mater. Chem.* **1999**, *9*, 2775.
- (24) (a) Mieczkowski, J.; Gomola, K.; Koseska, J.; Pocięcha, D.; Szydłowska, J.; Gorecka, E. *J. Mater. Chem.* **2003**, *13*, 2132. (b) Gorecka, E.; Vaupotic, N.; Pocięcha, D.; Cepic, M.; Mieczkowski, J. *Chem. Phys. Chem.* **2005**, *6*, 1087. (c) Pelzl, G.; Weissflog, W.; Baumeister, U.; Diele, S. *Liq. Cryst.* **2003**, *30*, 1151.
- (25) (a) Gorecka, E.; Pocięcha, D.; Araoka, F.; Link, D. R.; Nakata, M.; Thisayukta, J.; Takanishi, Y.; Ishikawa, K.; Watanabe, J.; Takezoe, H. *Phys. Rev. E* **2000**, *62*, 4524. (b) Nakata, M.; Link, D. R.; Thisayukta, J.; Takanishi, Y.; Ishikawa, K.; Watanabe, J.; Takezoe, H. *J. Mater. Chem.* **2001**, *11*, 2694.
- (26) (a) Link, D. R.; Natale, G.; Shao, R.; MacLennan, J. E.; Clark, N. A.; Korblova, E.; Walba, D. M. *Science* **1997**, *278*, 1924. (b) Walba, D. M.; Korblova, E.; Shao, R.; MacLennan, J. E.; Link, D. R.; Glaser, M. A.; Clark, N. A. *Science* **2000**, *288*, 2181.
- (27) Shen, D.; Pegenau, A.; Diele, S.; Wirth, I.; Tschierske, C. *J. Am. Chem. Soc.* **2000**, *122*, 1593.
- (28) (a) Takezoe, H.; Takanishi, Y. *Jpn. J. Appl. Phys.* **2006**, *45*, 597. (b) Accelli, I.; Prampolini, G. *Chem. Phys.* **2005**, *314*, 283. (c) Weissflog, W.; Nadasi, H.; Dunemann, U.; Pelzl, G.; Diele, S.; Eremin, A.; Kresse, H. *J. Mater. Chem.* **2001**, *11*, 2748.